

Rib waveguide as a three-mode demultiplexer for SOI

OMNIA M. NAWWAR,^{1,2,3,*}  JIDEFOR A. H. ODOEZE,¹  AND HOSSAM M. H. SHALABY^{1,2} 

¹Department of Electronics and Communications Engineering, Egypt-Japan University of Science and Technology (E-JUST), Alexandria 21934, Egypt

²Faculty of Engineering, Alexandria University, Alexandria 21544, Egypt

³Graduate School of Information Science and Electrical Engineering, Kyushu University, Fukuoka 819-0395, Japan

*omnia.nawwar@ejust.edu.eg

Abstract: A flying-bird mode-division demultiplexer (FBMDD) that can demultiplex three modes is proposed. The demultiplexer is simply a modified rib waveguide, called a j-rib, followed by three fan-out waveguides. The fan-out waveguides are three single-mode strip waveguides, attached to the center, right, and left regions of the j-rib waveguide. The input of the j-rib waveguide is excited by three modes, e.g., EH_{11} , EH_{12} , and EH_{13} . The waveguide is designed so as to separate the modes and guide them to the center, right, and left regions, respectively. The separated modes are then fanned-out to the output ports. A theoretical analysis of the proposed demultiplexer is developed based on extensions of the large single-mode rib conditions. In addition, both MODE and 3D-FDTD simulations of the demultiplexer are performed to validate the proposed concept. Our results reveal that the device has low insertion losses and crosstalks over a very wide bandwidth.

© 2018 Optical Society of America under the terms of the [OSA Open Access Publishing Agreement](#)

1. Introduction

The increasing bandwidth of future parallel chip multiprocessor, to meet up with current demand of high transmission rates, has been promising with the emergence of optical interconnect [1]. System capacity can be increased by the adoption of multiplexing techniques, e.g., wavelength-division multiplexing (WDM), space-division multiplexing (SDM), and mode-division multiplexing (MDM) [2,3]. However, SDM increases footprint as each signal has its own path [4]. Consequently, it is unsuitable for on-chip applications. WDM seems to be better than SDM techniques for on-chip application as it increases capacity without increasing footprint [5]. However, multiple sources are needed for different wavelengths. This would increase cost and complexity of WDM and make it unsuitable for on-chip applications.

On the other hand, MDM techniques can increase capacity without increasing the footprint, making them more suitable for on-chip applications [6–8]. A mode multiplexer/demultiplexer is one of the key components in any MDM system, accordingly many mode (de)multiplexers have been proposed in literature. Dai *et al.* have demonstrated experimentally a small silicon mode (de)multiplexer with cascaded asymmetrical directional couplers [9]. For a three mode multiplexer, the worst measured insertion loss (IL) is 0.5 dB with device length of 110 μm . Using 2 waveguides and a Bragg grating, Qui *et al.* have presented a silicon mode multi/demultiplexer based on multimode grating assisted couplers [10]. For three mode demultiplexing, the footprint is more than 400 μm and the worst simulated IL is 0.34 dB. Gui *et al.* have fabricated an on-chip two-mode multiplexer/demultiplexer using a tapered asymmetrical grating-assisted contra-directional coupler [11]. The device can demultiplex two modes with a footprint of more than 25 μm . Sun *et al.* have designed and fabricated a mode (de)multiplexer for 2 modes. It uses power splitters and adiabatic tapers for two mode multiplexing [12]. The on-chip footprint is

200 μm with worst measured IL of 1 dB. Dorin and Ye have designed and fabricated a two-mode silicon-on-insulator (SOI) ring resonator for MDM systems [13]. The ring radius is 20 μm and worst measured IL is 2.5 dB. Chen *et al.* have presented and fabricated silicon three-mode (de)multiplexer based on cascaded asymmetric Y junctions [14]. Shalaby has proposed a simple three mode-division (de)multiplexer using a bi-directional coupler (called BMDM) supported with a Bragg grating [15,16]. Nawwar *et al.* have fabricated the BMDM using only two strip waveguides and a Bragg grating [8]. The length of the device is only 18 μm with worst IL of -5.402 dB. Xu *et al.* have presented and fabricated an ultra-broadband 16-channel mode-division (de)multiplexer utilizing densely packed bent waveguide arrays [17]. Chang *et al.* have fabricated 3 mode (de)multiplexer based on asymmetric Y-junction with PhC-like SW structure using the inverse design method [7]. The footprint is less than 18 μm^2 with worst IL of 1 dB.

In this paper, we propose a new and simple mode-division demultiplexer using only one waveguide, followed by three fan-out waveguides. As our device structure mimics a flying bird, we call it a *flying-bird mode-division demultiplexer (FBMDD)*. The FBMDD is designed so as to separate three modes and guide them to the center (body), right wing, and left wing of the FBMDD. The separated modes are then fanned-out to the output waveguides. The demultiplexing is done using only one waveguide, which makes it competitive for on-chip application. Indeed, the device has a reduced footprint, yet it shows both low IL and crosstalks (CTs) over a very wide bandwidth.

The remaining of this paper is organized as follows. The structure of the proposed demultiplexer is described in Section 2. The theoretical analysis of the FBMDD and the mathematical derivations of corresponding conditions needed for optimum design are given in Section 3. Both MODE and 3D-FDTD simulations of proposed FBMDD are performed in Sections 4 and 5, respectively. The corresponding numerical results are presented in same sections as well. Finally, our concluding remarks are given in Section 6.

2. FBMDD structure

Figures 1(a) and 1(b) show the 3D perspective and cross-sectional views of proposed FBMDD in photonics integrated systems, respectively. The structure comprises of a modified rib waveguide, called *j-rib* [18], followed by three fan-out waveguides. The fan-out waveguides are three single-mode strip waveguides, attached to the center, right, and left regions of the *j-rib* waveguide. The input to the *j-rib* waveguide is excited by three modes, namely, EH_{11} , EH_{12} , and EH_{13} (we adopt the notation of HE_{pq} and EH_{pq} , any $p, q \in \{1, 2, 3, \dots\}$, for TE-like and TM-like modes,

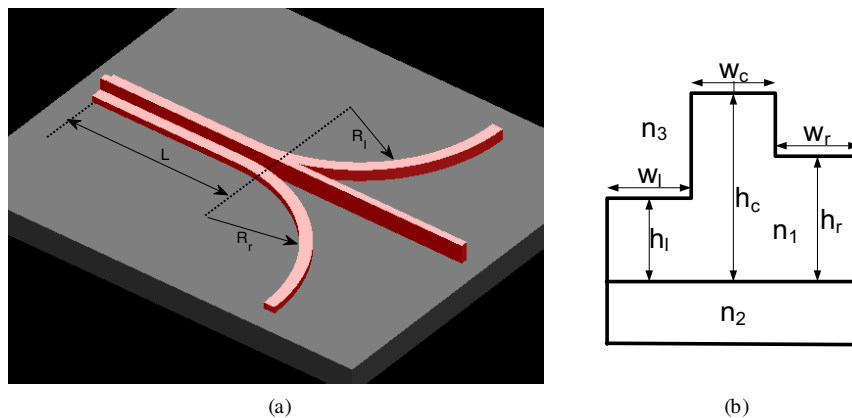


Fig. 1. Schematic configuration of flying-bird mode-division demultiplexer: (a) Perspective view; (b) Cross-sectional view.

respectively). The waveguide is designed so as to separate the modes and guide them to the center, right, and left regions, respectively. The separated modes are then fanned-out to the output ports. The length of the j -rib waveguide is L . The thicknesses of the center, right, and left regions are denoted by h_c , h_r , and h_l , respectively. The widths of the center, right, and left regions are denoted by w_c , w_r , and w_l , respectively. The radii of the right and left output curvatures are denoted by R_r and R_l , respectively.

3. Theoretical analysis

In this section, we aim at obtaining design equations to determine the dimensions of the geometrical structure of proposed device. We adopt the effective-index method (EIM), which has been proven to be in good agreement with full vectorial methods [19]. EIM depends on decomposing the structure into two (vertical and horizontal) 2D slab waveguides. The effective index n_{eff} of each slab waveguide is obtained by solving an eigenvalue equation. The eigenvalue equations for both TE and TM modes in an asymmetrical slab waveguide with thickness d are given by:

$$\begin{aligned} k_0 d \sqrt{n_1^2 - n_{\text{eff}}^2} - m\pi &= \tan^{-1} \left(\sqrt{\frac{n_{\text{eff}}^2 - n_2^2}{n_1^2 - n_{\text{eff}}^2}} \right) + \tan^{-1} \left(\sqrt{\frac{n_{\text{eff}}^2 - n_3^2}{n_1^2 - n_{\text{eff}}^2}} \right); \quad \text{for TE modes,} \\ k_0 d \sqrt{n_1^2 - n_{\text{eff}}^2} - m\pi &= \tan^{-1} \left[\left(\frac{n_1}{n_2} \right)^2 \sqrt{\frac{n_{\text{eff}}^2 - n_2^2}{n_1^2 - n_{\text{eff}}^2}} \right] + \tan^{-1} \left[\left(\frac{n_1}{n_3} \right)^2 \sqrt{\frac{n_{\text{eff}}^2 - n_3^2}{n_1^2 - n_{\text{eff}}^2}} \right]; \quad \text{for TM modes,} \end{aligned} \quad (1)$$

where n_1 , n_2 , and n_3 are the refractive indices of the waveguide core, buried oxide, and cladding respectively, $m \in \{0, 1, 2, \dots\}$ is the mode order, $k_0 = 2\pi/\lambda$ is the free-space propagation constant, and λ is the free-space optical wavelength. In our analysis in this section, we use approximate solutions to (1), as given in [20], to get the effective indices. In the next two subsections, we determine the effective indices in both vertical and horizontal slab waveguides, respectively.

3.1. Vertical solution of the structure

The heights h_c , h_r , and h_l are now seen as slab thicknesses of the center, right, and left vertical planar waveguides. Accordingly, the corresponding effective indices are given by:

$$\begin{aligned} n_{\text{eff}_c}^2(m) &\approx n_1^2 - (m+1)^2 \left(\frac{\pi}{k_0 h_{c,eq}} \right)^2 \\ n_{\text{eff}_r}^2(m) &\approx n_1^2 - (m+1)^2 \left(\frac{\pi}{k_0 h_{r,eq}} \right)^2 \\ n_{\text{eff}_l}^2(m) &\approx n_1^2 - (m+1)^2 \left(\frac{\pi}{k_0 h_{l,eq}} \right)^2, \end{aligned} \quad (2)$$

respectively, where, $m \in \{0, 1, 2, \dots\}$, $h_{c,eq} = h_c + Q/k_0$, $h_{r,eq} = h_r + Q/k_0$, and $h_{l,eq} = h_l + Q/k_0$. Here

$$Q = \begin{cases} \frac{1}{\sqrt{n_1^2 - n_2^2}} + \frac{1}{\sqrt{n_1^2 - n_3^2}}; & \text{for TE modes,} \\ \frac{(n_2/n_1)^2}{\sqrt{n_1^2 - n_2^2}} + \frac{(n_3/n_1)^2}{\sqrt{n_1^2 - n_3^2}}; & \text{for TM modes.} \end{cases} \quad (3)$$

3.2. Horizontal solution of the structure

Here, the widths w_c , w_r , and w_l are now seen as slab thicknesses of the center, right, and left horizontal planar waveguides. The effective indices of the various modes in the center and right regions of the FBMDD can be obtained from:

$$\begin{aligned}
 N_{wgc}^2(\ell, m) &\approx n_{\text{eff}_c}^2(m) - (\ell + 1)^2 \left(\frac{\pi}{k_0 w_{c,eq}(m)} \right)^2 \\
 N_{wgr}^2(\ell, m) &\approx n_{\text{eff}_r}^2(m) - (\ell + 1)^2 \left(\frac{\pi}{k_0 w_{r,eq}(m)} \right)^2 \\
 N_{wgl}^2(\ell, m) &\approx n_{\text{eff}_l}^2(m) - (\ell + 1)^2 \left(\frac{\pi}{k_0 w_{l,eq}(m)} \right)^2
 \end{aligned} \tag{4}$$

where $\ell, m \in \{0, 1, 2, \dots\}$, $w_{c,eq}(m) = w_c + R_c(m)/k_0$, $w_{r,eq}(m) = w_r + R_r(m)/k_0$, and $w_{l,eq}(m) = w_l + R_l(m)/k_0$. Here $R_c(m)$, $R_r(m)$, and $R_l(m)$ are given by:

$$\begin{aligned}
 R_c(m) &= \begin{cases} \frac{1}{\sqrt{n_{\text{eff}_c}^2(m) - n_{\text{eff}_r}^2(m)}} + \frac{1}{\sqrt{n_{\text{eff}_c}^2(m) - n_{\text{eff}_l}^2(m)}}; & \text{for TE modes,} \\ \frac{(n_{\text{eff}_r}(m)/n_{\text{eff}_c}(m))^2}{\sqrt{n_{\text{eff}_c}^2(m) - n_{\text{eff}_r}^2(m)}} + \frac{(n_{\text{eff}_l}(m)/n_{\text{eff}_c}(m))^2}{\sqrt{n_{\text{eff}_c}^2(m) - n_{\text{eff}_l}^2(m)}}; & \text{for TM modes,} \end{cases} \\
 R_r(m) &= \begin{cases} \frac{1}{\sqrt{n_{\text{eff}_r}^2(m) - n_{\text{eff}_c}^2(m+1)}} + \frac{1}{\sqrt{n_{\text{eff}_r}^2(m) - n_3^2}}; & \text{for TE modes,} \\ \frac{(n_{\text{eff}_c}(m+1)/n_{\text{eff}_r}(m))^2}{\sqrt{n_{\text{eff}_r}^2(m) - n_{\text{eff}_c}^2(m+1)}} + \frac{(n_3/n_{\text{eff}_r}(m))^2}{\sqrt{n_{\text{eff}_r}^2(m) - n_3^2}}; & \text{for TM modes,} \end{cases} \\
 R_l(m) &= \begin{cases} \frac{1}{\sqrt{n_{\text{eff}_l}^2(m) - n_{\text{eff}_c}^2(m+2)}} + \frac{1}{\sqrt{n_{\text{eff}_l}^2(m) - n_3^2}}; & \text{for TE modes,} \\ \frac{(n_{\text{eff}_c}(m+2)/n_{\text{eff}_l}(m))^2}{\sqrt{n_{\text{eff}_l}^2(m) - n_{\text{eff}_c}^2(m+2)}} + \frac{(n_3/n_{\text{eff}_l}(m))^2}{\sqrt{n_{\text{eff}_l}^2(m) - n_3^2}}; & \text{for TM modes.} \end{cases}
 \end{aligned} \tag{5}$$

3.3. Mode confinement

In this subsection, we derive mathematical expressions for the conditions needed to separate and confine input modes into the three regions of the FMDD. Using our aforementioned notation, we notice that $q \equiv m + 1$ and $p \equiv \ell + 1$.

3.3.1. Confinement of the fundamental mode in the center

Here, we wish to find the conditions so that only the fundamental mode (HE_{11} or EH_{11}) is confined/kept in the center region. Of course this is exactly the same as that of large single-mode rib waveguides [21]. Specifically, two conditions should be satisfied in both vertical and horizontal directions.

Vertical condition Given any $p \in \{1, 2, 3, \dots\}$, first we need HE_{p1} or EH_{p1} to be confined in the center region. This is satisfied if $n_{\text{eff}_c}(0) > n_{\text{eff}_r}(0)$. Next, we need higher-order vertical modes, HE_{pq} or EH_{pq} , $q \in \{2, 3, 4, \dots\}$, to leak away from the center to other regions. This is satisfied if

$n_{\text{eff}_c}(1) < n_{\text{eff}_l}(0)$. Using (2), the last two conditions reduce to:

$$1/2 < s_r < 1, \quad (6)$$

where $s_r \stackrel{\text{def}}{=} h_{r,eq}/h_{c,eq}$.

Horizontal condition To keep only the fundamental mode (HE₁₁ or EH₁₁) in the center region, a horizontal condition should be satisfied as well, that is we leak out higher-order horizontal modes ($p \geq 2$) into other regions by making $N_{\text{wg}_c}(1, 0) < n_{\text{eff}_r}(0)$. Using (2) and (4), this condition reduces to:

$$t_c < 2 \frac{s_r}{\sqrt{1 - s_r^2}}, \quad (7)$$

where $t_c \stackrel{\text{def}}{=} w_{c,eq}(0)/h_{c,eq}$.

3.3.2. Confinement of first-order mode to the right

Here, we wish to find the conditions so that only the first-order mode (HE₁₂ or EH₁₂) is confined in the right region.

Vertical condition Given any $p \in \{1, 2, 3, \dots\}$, first we need HE_{p2} or EH_{p2} to be confined in the right. This is satisfied if $n_{\text{eff}_c}(1) > n_{\text{eff}_l}(0)$. Next, we need HE_{pq} or EH_{pq}, $q \in \{3, 4, 5, \dots\}$, to leak away from the right to left region (obviously it cannot stay in the center as it does not satisfy (6)). This is satisfied if $n_{\text{eff}_c}(2) < n_{\text{eff}_l}(0)$. Using (2), the last two conditions reduce to:

$$1/3 < s_l < 1/2, \quad (8)$$

where $s_l \stackrel{\text{def}}{=} h_{l,eq}/h_{c,eq}$.

Horizontal condition To keep only the first-order mode (HE₁₂ or EH₁₂) in the right region, we leak out higher-order horizontal modes ($p \geq 2$) into other regions (e.g., left) by making $N_{\text{wg}_r}(1, 0) < n_{\text{eff}_l}(0)$. Using (2) and (4), this condition reduces to:

$$t_r < 2 \frac{s_r s_l}{\sqrt{s_r^2 - s_l^2}}, \quad (9)$$

where $t_r \stackrel{\text{def}}{=} w_{r,eq}(0)/h_{c,eq}$.

3.3.3. Confinement of second-order mode to the left

Here, we wish to find the conditions so that only the second-order mode (HE₁₃ or EH₁₃) is confined in the left region.

Vertical condition Given any $p \in \{1, 2, 3, \dots\}$, we need HE_{p3} or EH_{p3} to be confined in the left. This is already satisfied by condition (8).

Horizontal condition To keep only the second-order mode (HE₁₃ or EH₁₃) in the left region, we select its width so as to maximize the overlap between the electric field of second-order mode in the center region with that of fundamental mode in the left region.

One should notice that the condition in Subsection 3.3.2 above would increase the crosstalks in the left region a bit. In order to reduce the crosstalks in this region, one can add an extra region of height h_{grd} to the leftmost of the device. This region might be called a *ground region*.

All unwanted higher-order modes would leak away to this ground region. The corresponding horizontal condition in this case is:

$$t_l < \frac{2s_l s_{\text{grd}}}{\sqrt{s_l^2 - s_{\text{grd}}^2}}, \quad (10)$$

where $t_l \stackrel{\text{def}}{=} w_{l,eq}(0)/h_{c,eq}$, $s_{\text{grd}} \stackrel{\text{def}}{=} h_{\text{grd},eq}/h_{c,eq}$, and $h_{\text{grd},eq} = h_{\text{grd}} + Q/k_0$. Here, h_{grd} denotes the height of the ground region and the vertical condition leads to $1/4 < s_{\text{grd}} < 1/3$. In this paper, we do not consider the ground region in our structure.

4. Simulation with MODE solution

In this section, we validate our proposed concept using MODE solution on a j-rib waveguide. The operating wavelength is $\lambda = 1550$ nm and the refractive indices are $n_1 = 3.473$, $n_2 = 1.444$, and $n_3 = 1.444$. The dimensions of the waveguide can be obtained using analytical results of Section 3 as: $h_c = 1.4$ μm , $h_r = 0.7$ μm , $h_l = 0.62$ μm , $w_c = 0.8$ μm , $w_r = 1.2$ μm , and $w_l = 1.4$ μm . These dimensions satisfy the conditions (6), (7), (8), and (9) for HE (TE-like) modes with $s_r = 0.550187$, $t_c = 1.198378$, $s_l = 0.498780$, and $t_r = 1.452988$. It should be noticed that the selection of suitable dimensions is robust. Indeed, the acceptable dimensions lie in a large domain as given by (6), (7), (8), and (9). This makes the device fabrication tolerant with robust performance.

Using these dimensions, we simulate the structure and get cross-sectional electric field distributions for first three TE-like modes, specifically HE₁₁, HE₁₂, and HE₁₃. These have mode numbers 1, 3, and 4, respectively. The results of the MODE simulation are plotted in Fig. 2. It is clear from the figure that all three modes are confined properly in the center, right, and left regions. One can see from Fig. 2(c) that the crosstalks are more in the case of HE₁₃. This is due to the leak of higher-order modes to the left region, as discussed in Subsection 3.3.2 above. The crosstalks in this case can be reduced by adding an extra region, to which all higher-order modes would leak away.

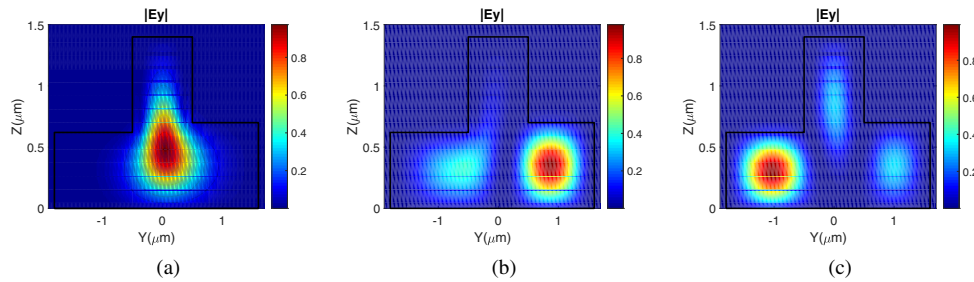


Fig. 2. Cross-sectional electric field distributions for first three TE-like modes (HE₁₁, HE₁₂, and HE₁₃) using MODE simulation.

Using same dimensions, we also simulate the structure for first three TM-like modes, specifically EH₁₁, EH₁₂, and EH₁₃. These have mode numbers 2, 5, and 6, respectively. The results are shown in Fig. 3. The figure indicates similar conclusions to that of TE-like modes. However, Fig. 3(c) indicates that the crosstalks in the case of EH₁₃ are increased compared to that in case of HE₁₃ in Fig. 2(c). This is because the dimensions of the structure are optimized according to the conditions of HE modes and not EH modes.

From above discussion, it is perceived that the existence of aforementioned modes with proper confinement in different regions confirms the feasibility of achieving the demultiplexing process using the proposed device. This also introduces a new concept about the possibility of constructing a mode-division demultiplexer using only one waveguide.

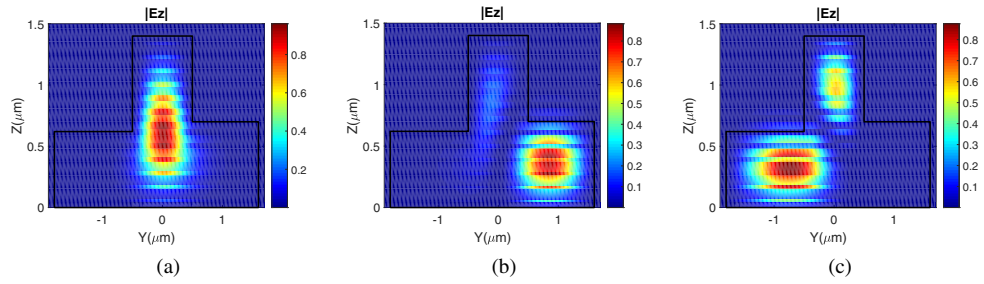


Fig. 3. Cross-sectional electric field distributions for first three TM-like modes (EH_{11} , EH_{12} , and EH_{13}) using MODE simulation.

5. Simulation with 3D-FDTD solution

In this section, we perform 3D-FDTD simulations on the propagation of three EH modes in an FBMDD with same refractive indices and operating wavelength as given in last section. We use mode-expansion monitors to determine both the IL and CTs of each mode. First, we design a multimode input strip waveguide (with dimension $0.25 \mu\text{m} \times 1.4 \mu\text{m}$) that supports three EH (TM-like) modes, namely EH_{11} , EH_{12} , and EH_{13} . The electric field profiles of these modes are shown in Fig. 4. The strip waveguide would inject the modes into an FBMDD for demultiplexing. Using derived conditions of Section 3, we get the dimensions of the FBMDD in relation to the dimensions of the multi-mode input waveguide as follows: $h_c = 1.4 \mu\text{m}$, $h_r = 0.85 \mu\text{m}$, $h_l = 0.49 \mu\text{m}$, $w_c = 0.25 \mu\text{m}$, $w_r = 0.4 \mu\text{m}$, and $w_l = 0.4 \mu\text{m}$. These dimensions satisfy the conditions (6), (7), (8), and (9) for EH (TM-like) modes with $s_r = 0.614577$, $t_c = 0.764798$, $s_l = 0.362300$, and $t_r = 0.752723$. In addition, we select $L = 13.9 \mu\text{m}$, and $R_r = R_l = 5 \mu\text{m}$ for best performance.

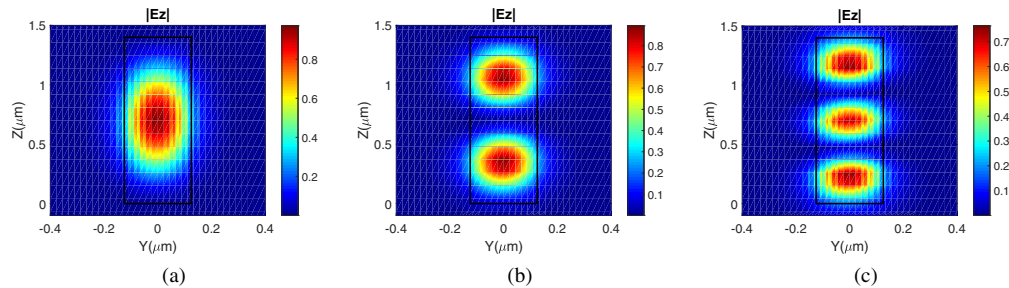


Fig. 4. Electric field profiles of input waveguide when excited with TM-like modes: (a) EH_{11} , (b) EH_{12} , and (c) EH_{13} .

5.1. Propagation in the FBMDD when excited with EH_{11} , EH_{12} , and EH_{13} modes

We excite the FBMDD with EH_{11} , EH_{12} , and EH_{13} modes separately and get the results of the propagation through the structure.

The corresponding electric field profiles of the output waveguides from FBMDD are shown in Fig. 5.

One can notice that although EH_{12} and EH_{13} have two and three peaks, respectively, the corresponding outputs seen in the FBMDD have only one peak. Indeed, based on the theoretical analysis given in section 3, these modes leak/couple to fundamental modes in the right and left wings, respectively. It is also clear that the field of fundamental mode in right region (Fig. 3(b)) has a good overlap with the lower lobe of the field of first-order mode in the center (Fig. 4(b)).

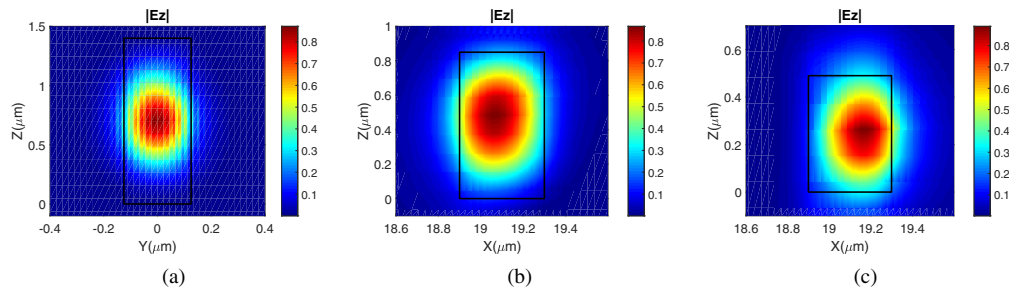


Fig. 5. Electric field profiles of output waveguides from FBMD when excited with TM-like modes: (a) EH_{11} , (b) EH_{12} , and (c) EH_{13} .

Similarly, the field of fundamental mode in left region (Fig. 3(c)) has a good overlap with the lower lobe of the field of second-order mode in the center (Fig. 4(c)). One more remark is that the horizontal axes in Figs. 5(b) and 5(c) are labeled by X , not Y . Clearly, this is because after splitting from the left and right regions, the wings of the device has perpendicular orientations to its main body, Fig. 1(a).

In addition, the absolute-squared values of each mode, while propagating in FBMD, are shown in Fig. 6. The blue regions indicate the minimum levels and the red regions indicate the maximum levels. The in-continuity in the field represents successive peaks and valleys of the field along the x -direction. The image shows that the proposed FBMD successfully separates the EH_{11} , EH_{12} , and EH_{13} modes into center body, left wing, and right wing, respectively, with good insertion losses and crosstalks.

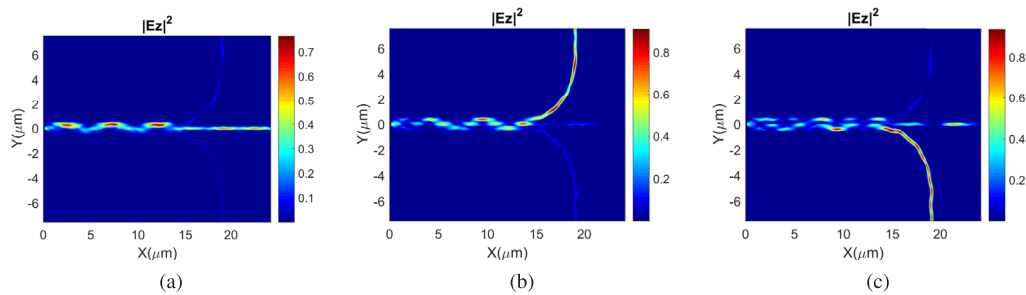


Fig. 6. Propagation of modes inside an FBMD: (a) EH_{11} , (b) EH_{12} , and (c) EH_{13} .

5.2. Insertion losses and crosstalks

In this subsection, the resulting insertion losses and crosstalks are plotted versus wavelength in Fig. 7. Figures 7(a), 7(b), and 7(c) show the results when exciting the demultiplexer by EH_{11} , EH_{12} , and EH_{13} modes, respectively.

It is clear from the figure that the three modes are separated at the three ports with suitable values of insertion losses and crosstalks. Specifically, at a wavelength of 1550 nm, the insertion losses are about -1.62 dB, -2.26 dB, and -3.4 dB when exciting the FBMD by EH_{11} , EH_{12} , and EH_{13} modes, respectively. In addition, the crosstalks are below -11.8 dB, -12.2 dB, and -11.8 dB for these modes, respectively. It is also clear from the figures that the 3 dB bandwidth of the proposed device is more than 160 nm. The high bandwidth of the device and its robust selectivity of dimensions make it fabrication tolerant against dimensions' variations.

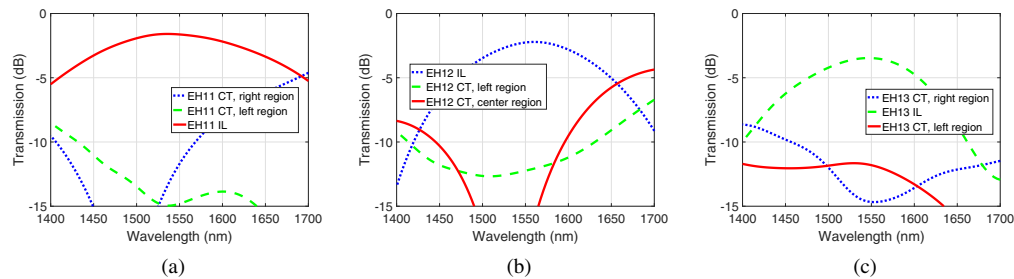


Fig. 7. 3D-FDTD simulation of both insertion losses and crosstalks versus wavelength of proposed FBMD when excited by: (a) EH_{11} , (b) EH_{12} , and (c) EH_{13} modes.

6. Conclusion

A flying-bird mode-division demultiplexer (FBMD), based on a modified rib waveguide, called j-rib, has been proposed. It can demultiplex three modes simultaneously. The proposed structure introduces a new perception about the possibility of constructing a mode-division demultiplexer using only one waveguide. The concept has been tested by attaching a multimode strip waveguide, carrying three different modes, e.g., EH_{11} , EH_{12} , and EH_{13} , to the input of the j-rib waveguide. Three fan-out strip waveguides are attached to the center, right, and left regions of the j-rib waveguide to guide out the demultiplexed modes. These modes have been properly separated to the body (center) and wings (right and left) of the FBMD. A theoretical analysis of the proposed demultiplexer is developed based on extensions of the large single-mode rib conditions. In addition, both MODE and 3D-FDTD simulations of proposed demultiplexer have been performed to prove the validity of the proposed concept. At a J-Rib length of $13.9 \mu\text{m}$, our results show good insertion losses and crosstalks over a very wide 3 dB bandwidth of about 160 nm.

References

1. K. Bergman, L. Carloni, A. Biberman, J. Chan, and G. Hendry, *Photonic Network-on-Chip Design* (Springer, 2014).
2. P. J. Winzer and G. J. Foschini, "MIMO capacities and outage probabilities in spatially multiplexed optical transport systems," *Opt. Express* **19**(17), 16680–16696 (2011).
3. P. J. Winzer, "Modulation and multiplexing in optical communications," in *Conference on Lasers and Electro-Optics/International Quantum Electronics Conference*, (Optical Society of America, 2009), p. CTuL3.
4. S. Berdagu  and P. Facq, "Mode division multiplexing in optical fibers," *Appl. Opt.* **21**(11), 1950–1955 (1982).
5. L.-W. Luo, N. Ophir, C. P. Chen, L. H. Gabrielli, C. B. Poitras, K. Bergmen, and M. Lipson, "WDM-compatible mode-division multiplexing on a silicon chip," *Nat. Commun.* **5**(1), 3069 (2014).
6. B. Stern, X. Zhu, C. P. Chen, L. D. Tzuang, J. Cardenas, K. Bergman, and M. Lipson, "On-chip mode-division multiplexing switch," *Optica* **2**(6), 530–535 (2015).
7. W. Chang, L. Lu, X. Ren, D. Li, Z. Pan, M. Cheng, D. Liu, and M. Zhang, "Ultra-compact mode (de)multiplexer based on subwavelength asymmetric Y-junction," *Opt. Express* **26**(7), 8162–8170 (2018).
8. O. M. Nawwar, H. M. Shalaby, and R. K. Pokharel, "Modeling, simulation, and fabrication of bi-directional mode-division multiplexing for silicon-on-insulator platform," *Appl. Opt.* **57**(1), 42–51 (2018).
9. D. Dai, J. Wang, and Y. Shi, "Silicon mode (de)multiplexer enabling high capacity photonic networks-on-chip with a single-wavelength-carrier light," *Opt. Lett.* **38**(9), 1422–1424 (2013).
10. H. Qiu, H. Yu, T. Hu, G. Jiang, H. Shao, P. Yu, J. Yang, and X. Jiang, "Silicon mode multi/demultiplexer based on multimode grating-assisted couplers," *Opt. Express* **21**(15), 17904–17911 (2013).
11. C. Gui, Y. Gao, Z. Zhang, and J. Wang, "On-chip silicon two-mode (de)multiplexer for OFDM/OQAM data transmission based on grating-assisted coupler," *IEEE Photon. J.* **7**(6), 1–7 (2015).
12. C. Sun, Y. Yu, M. Ye, L. Shi, and X. Zhang, "An integrated mode (de)multiplexer based on adiabatic couplers," in *Conference on Lasers and Electro-Optics*, (Optical Society of America, 2016), p. SM1F.7.
13. B. A. Dorin and W. N. Ye, "Two-mode division multiplexing in a silicon-on-insulator ring resonator," *Opt. Express* **22**(4), 4547–4558 (2014).
14. W. Chen, P. Wang, T. Yang, G. Wang, T. Dai, Y. Zhang, L. Zhou, X. Jiang, and J. Yang, "Silicon three-mode (de)multiplexer based on cascaded asymmetric y junctions," *Opt. Lett.* **41**(12), 2851–2854 (2016).
15. H. M. H. Shalaby, "Bi-directional coupler as a mode-division multiplexer/demultiplexer," *J. Lightwave Technol.* **34**(15), 3633–3640 (2016).

16. H. M. H. Shalaby, "Bidirectional mode-division multiplexers with antireflection gratings," *Appl. Opt.* **57**(3), 476–484 (2018).
17. H. Xu and Y. Shi, "Ultra-broadband 16-channel mode division (de)multiplexer utilizing densely packed bent waveguide arrays," *Opt. Lett.* **41**(20), 4815–4818 (2016).
18. J. A. Odoeze, H. M. H. Shalaby, and M. O. Nawwar, "J-rib waveguide as a mode-division demultiplexer," in *Asia Communications and Photonics Conference 2016*, (Optical Society of America, 2016), p. AF1G.6.
19. M. D. G. Mihail and M. Dumitrescu, "Effective index method for computation of the propagation constant and electromagnetic field distribution in z-uniform dielectric or semiconductor waveguides," in *Fifth Conference on Optics, 1998*, (Proc. SPIE 3405, ROMOPTO '97, 1998), p. 922.
20. S. P. Pogossian, "A new approach to determining the waveguide mode index distribution," *Opt. Quantum Electron.* **25**(6), 417–422 (1993).
21. S. P. Pogossian, L. Vescan, and A. Vonsovici, "The single-mode condition for semiconductor rib waveguides with large cross section," *J. Lightwave Technol.* **16**(10), 1851–1853 (1998).